ACS OMEGA

Open Access

http://pubs.acs.org/journal/acsodf

Article

Integration of Lipid-Functionalized Epigallocatechin-3-gallate into PLGA Matrix as a Novel Polyphenol-Based Nanoantioxidant

Cristina Minnelli, Pierluigi Stipa, Giovanna Mobbili, Simona Sabbatini, Brenda Romaldi, Tatiana Armeni, and Emiliano Laudadio*

Cite This: *ACS Omega* 2023, 8, 48292−48303

Read Online

ACCESS | Metrics & More | Article Recommendations

ABSTRACT: The search for polyphenol-based materials with antioxidant activity is a growing research area in the biomedical field. To obtain an efficient and stable nanoantioxidant, a novel biosystem was designed by integrating a lipophilic derivative of epigallocatechin-3-gallate (named EGCG-C18) on the surface of poly(lactic-*co*-glycolic acid) (PLGA). Poly(vinyl alcohol) (PVA) and 1,2-distearoyl-*sn*-glycero-3-phosphoethanolamine-poly(ethylene glycol) (DSPE-PEG_{2000}) were selected as polymeric and lipidic stabilizers, respectively, and their influence on both physical properties and the antioxidant activity of nanoantioxidant was investigated by a combined in silico and experimental approach. Full-atom molecular dynamics (MD) simulations were carried out to describe the different self-assembly processes of all components and the interactions that guided the EGCG-C18 insertion inside the PLGA matrix. Together with infrared spectroscopy results, the formation of an antioxidant lipid shell on the PLGA surface was clear. Dynamic light scattering and transmission electron microscopy showed that in the presence of DSPE-PEG_{2000}, NPs were smaller than those treated with PVA. In addition, the different stabilizers used strongly influenced the ROS-scavenging ability of nanomaterials and this effect was strictly related to the molecular organization of EGCG-C18. MD showed that the apolar interaction between the alkyl chains of DSPE-PEG_{2000} and EGCG-C18 oriented the phenolic groups of the polyphenol toward the solvent, providing an ability of NP to scavenge hydroxyl radicals over to free EGCG-C18 and PLGA/PVA NPs. Finally, the ability of nanoantioxidants to protect human dermal fibroblasts from cell death induced by oxidative stress has been tested, revealing the high potential of these novel NPs as polyphenol-based materials.

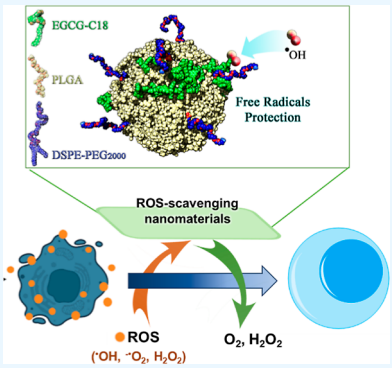

1. INTRODUCTION

The development of newly polyphenol-based materials represents a growing research area within biomedical science owing to many advantages related to the use of nanomaterials including enhanced chemical stability and bioavailability of the transported bioactive molecule.[1] These antioxidant nanomaterials, also called nanoantioxidants, act as effective scavengers of free radicals showing potential therapeutic applications in treating oxidative stress-related conditions, promoting wound healing and tissue generation.[2,3] The FDA-approved poly(lactic-*co*-glycolic acid) (PLGA) is an aliphatic copolymer polyester which received great attention for developing nanoantioxidants, given its biocompatibility and biodegradability. This is true since PLGA is suitable for the development of long-acting formulations owing to its proven biocompatible and biodegradable properties;[4] moreover, other advantages correlated to the use of this copolymer are the sustained releases including decreased dosing frequency, reduced side effects, and maintenance of stable level of the antioxidant plasma concentration.[5]

Although PLGA-nanoparticle (NP) carriers exhibited great potential, the lack of specific regulatory guidelines for the characterization of these materials counteracts their clinical uses and commercialization potential. In fact, its hydrophobicity could reduce the loading capacity of highly hydrophilic polyphenols such as epigallocatechin-3-gallate (EGCG) which is one of the most powerful antioxidants known. In this context, although PLGA nanoparticles improve the bioavailability and the beneficial effects of EGCG, their loading capacity was in the range of 5−10%.[6,7] Recently, we designed and synthesized a novel lipophilic EGCG derivative by covalently bonding a hydrocarbon chain (C18) at the OH group in para position of the gallate moiety (Figure 1).[8] This novel lipidic antioxidant, called EGCG-C18, strongly interacts with the lipophilic environment and shows ability to protect cells from oxidative stress over to EGCG. Moreover, the presence of the alkyl chain seems to also increase the chemical

Received: October 2, 2023
Revised: November 16, 2023
Accepted: November 17, 2023
Published: December 7, 2023

https://doi.org/10.1021/acsomega.3c07637
ACS Omega 2023, 8, 48292−48303

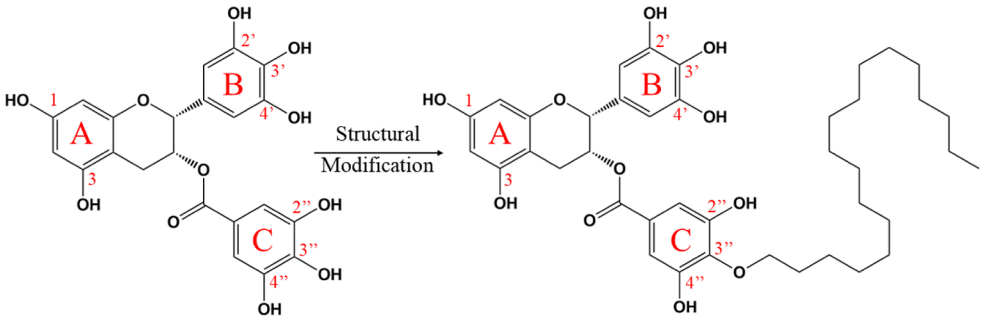

Figure 1. Chemical structure of EGCG and EGCG-C18.

stability of EGCG,[9,10] making this compound particularly interesting for the development of novel nanomaterials.

In this context, a self-assembly method was used to integrate the EGCG-C18 on the surface of the PLGA nanoparticle (NP) in the presence of two different stabilizers while looking for the construction of the most efficient and stable polyphenol-based nanoantioxidant. Poly(vinyl alcohol) (PVA) and 2-distearoyl-*sn*-glycero-3-phosphoethanolamine-poly(ethylene glycol) (DSPE-PEG_{2000}) were used as polymeric and lipidic stabilizers, respectively. Their influence on the PLGA NP's properties was deeply investigated using an integrated in silico and in vitro approach. Full-atom molecular dynamics (MD) simulations were carried out to describe the different self-assembly processes of components and the interactions that guided the EGCG-C18 insertion inside the PLGA matrix. Attenuated total reflectance−Fourier transform infrared (ATR-FTIR) spectroscopy confirmed the formation of an antioxidant lipid shell on the PLGA surface. Dynamic light scattering (DLS) and scanning electron microscopy (SEM) showed that in the presence of DSPE-PEG_{2000}, NPs were smaller than those treated with PVA underlining the high prediction potential of the in silico studies. The insertion of EGCG-C18 with the PLGA matrix in the presence of each stabilizer was evaluated by EGCG-C18-loaded experimental measurements and in silico calculation of the binding free energy. The NP's antioxidant scavenging activity against hydroxyl radicals ($OH^{\bullet}$) was studied by means of electron paramagnetic resonance (EPR) spectroscopy,[11] highlighting the important role of DSPE-PEG_{2000} on the orientation of the phenolic headgroup of EGCG-C18 toward the aqueous solution. Finally, the potential of NPs to protect human dermal fibroblasts from cell death induced by oxidative stress has been evaluated, revealing the high potential of these novel NPs as polyphenol-based nanoantioxidants.

Overall, the combined use of experimental and computational techniques provided important information about the behavior of both PLGA NPs alone and with the EGCG-C18 lipid shell, yielding useful guidelines for the successful production of complex polyphenol-based nanomaterial to be used for the treatment of pathologies associated with oxidative stress.

2. MATERIALS AND METHODS

2.1. Preparation of Polyphenol-Based PLGA NPs. PLGA−PVA NPs (PNPs) and PLGA-DSPE-PEG_{2000} NPs (DNPs) were prepared by using the single emulsification-solvent evaporation (ESE) method.[6] First, 20 mg of PLGA was dissolved in 6 mL of acetone (organic phase), and then, it was added dropwise to 6 mL of aqueous solution (water phase) containing 1% PVA or 2% DSPE-PEG_{2000} that acts as a surfactant for PNPs and DNPs, respectively. When the mixture of a volatile nonwater miscible solvent and an aqueous solution was formed, it was emulsified by sonication using an ultrasonicator (Qsonica Q125) at 30% amplitude for 30 s. The obtained oil-in-water emulsion was magnetically stirred for 24 h with a subsequent solvent evaporation step using a rotary evaporator for 2 h at 40 °C. Following NP preparation, unpurified suspensions were washed in distilled water two times at 25,000*g* for 20 min at 4 °C to remove the excess of PVA and/or DSPE-PEG_{2000}. EGCG-C18 was synthetized following our previous work[8] and then used to functionalize PNP and DNP on their surface by the single-step method;[12,13] the PLGA polymer and the EGCG-C18 lipid were either dissolved in acetone and added to an aqueous phase containing 1% PVA or 2% DSPE-PEG_{2000} followed by the same protocol used for the preparation of nonfunctionalized NPs. Six different systems were prepared: (i) free PLGA with PVA (PNP), (ii) PLGA/EGCG-C18 with PVA and 1:5 w/w ratio (NP-L2), (iii) PLGA/EGCG-C18 with PVA and 1:2 w/w ratio (NP-L3), (iv) PLGA/DSPE-PEG2000 1:50 w/w ratio (DNP), and other two systems where EGCG-C18 was added at 1:5 (v) and 1:2 ratio (vi) with respect to the PLGA matrix (DNP-L2 and DNP-L3, respectively).

The EGCG-C18 that did not interact with the PLGA surface was removed by gel exclusion chromatography following a well-established procedure.[6,14] The percentage of EGCG-C18 loaded inside the NP (drug loading, %) and its encapsulation efficiency (EE, %) inside all formulations were determined by the measurement of EGCG-C18 concentration in purified and impurified nanoparticles by the Folin−Ciocalteu assay as previously described.[8] All experiments were repeated at least three times, and measurements were carried out in triplicate. The EE % and drug loading % were calculated using the following relationships

$$\text{EE}\ (\%) = 100\times[\text{amount of EGCG} - \text{C18 inside nanoparticles/initial amount of EGCG} - \text{C18 added}]$$

$$\text{drug loading}\ (\%) = 100 \times [\text{amount of EGCG} - \text{C18 inside nanoparticles/total weight of nanoparticles}]$$

2.2. NP Characterization. *2.2.1. Dynamic Light Scattering.* The intensity-based diameter (*Z*-average) and the polydispersity index (PDI) of PLGA NP formulations were measured by dynamic light scattering (DLS) and electro-

https://doi.org/10.1021/acsomega.3c07637
ACS Omega 2023, 8, 48292−48303

phoretic light scattering using Malvern Zetasizer Nano ZS (Malvern Instruments GmbH, Marie-Curie-Straβe 4/1, 71,083 Herrenberg, Germany). Measurements were performed at 25 °C with a fixed angle of 173° in PBS at pH 7.4. The reported data represent the average of at least three different autocorrelations that were carried out for each sample.

2.2.2. Scanning Electron Microscopy. Scanning electron microscopy (SEM) measurements were performed by means of a Zeiss Supra 40 field emission electron microscope operating at 5 kV using the secondary electron signal from the "in lens" detector. Sample preparation consisted of dispersing a single droplet of solution on a polycarbonate filter followed by vacuum drying. Gold coating by sputtering was carried out after drying to avoid charging effects during the SEM observations. Samples were observed immediately after preparation. The acceleration voltage used for the SEM imaging was 5 kV by using an InLens sensor for secondary electron detection.

2.2.3. ATR-FTIR Measurements. IR spectra were acquired in reflectance mode using a PerkinElmer Spectrum GX1 spectrometer using the ATR accessory equipped with a ZnSe crystal. The spectral range was 4000−550 cm^{-1}, with a spectral resolution of 4 cm^{-1}; each spectrum was the result of 32 scans. Samples were placed directly onto the ZnSe crystal without any preparation. Then, five IR spectra were acquired for each sample. The average absorbance spectrum and the corresponding standard deviation spectra (average absorbance spectrum ± standard deviation spectra) were calculated before each sample acquisition; the background spectrum was collected on the clean crystal under the same conditions. Raw IR spectra were converted in absorbance mode and vector normalized (Spectrum 10.4.0 software, PerkinElmer). These spectra were curve-fitted in the 1800−1400 cm^{-1} spectral range; the number and the position of the underlying bands were also identified by second derivative minima analysis and fixed during the peak-fitting procedure with Gaussian functions.

2.2.4. In Vitro EGCG-C18 Release. The in vitro EGCG-C18 release from PNPs and DNPs was studied by the dialysis method after separation of unloaded polyphenol by gel-filtration chromatography following the same protocol used for the determination of encapsulation efficiency in Section 2.1. Briefly, 5 mL of NP suspension or EGCG-C18 alone was placed in the dialysis bag (12,000 MW cut off) and dialyzed against 50 mL of PBS (pH 7.4) with 40% (V/V) methanol. At scheduled intervals, 0.3 mL of the released medium was collected for analysis followed by the addition of the same volume of fresh 40% methanol in PBS to maintain a constant release volume. The cumulative percentage of EGCG-C18 release was quantified by the Folin−Ciocalteu assay as previously described.[8] Drug release was monitored for 96 h. The data reported represent the average of three experiments.

2.3. Computational Approach. With the aim to model systems as close as possible to the experimental conditions, 7500 lactic acid (LA) units in racemic forms were modeled and added to 2500 glycolic acid (GA) units, generating a 75/25 (LA/GA) PLGA copolymer. The random composition of PLGA with 75% PLA and 25% PGA was chosen to generate polymeric systems at the nanoscale level, in accordance with the experimental approaches used in this study.[15] The three-dimensional structures of EGCG-C18 and DSPE-PEG_{2000} molecules were generated and minimized using the semi-empirical AM1-BCC method.[16]

Six simulation boxes of 52 × 52 × 52 nm were prepared including one PLGA disperse system and 896,452 water molecules[17] in each box. Then, 32 and 94 EGCG-C18 molecules were randomly included in systems ii, iii, v, and vi, to reach the 1:5 and 1:2 w/w ratios, and 6 DSPE-PEG_{2000} molecules were added to simulate the 1:50 w/w ratio in systems iv, v, and vi.

GROMACS 5.1.1 suite[18,19] was used for MD simulations, while CHARMM36 force field[20] was chosen for calculations. All six systems were first minimized applying periodic box conditions (PBCs) in all directions. Each system was subjected to the steepest descent algorithm, and then, the final frame of minimization was used as the input structure for further minimization runs based on the conjugate gradient algorithm.[21] The Verlet cutoff scheme was used together with the LINCS algorithm for the constraints.[22]

An equilibration step based on 5 ns of annealing simulations was performed. Also in this case, the Verlet cutoff scheme and the LINCS algorithm were used, together with the particle mesh Ewald (PME) method for the treatment of the long-range interactions. A weak temperature coupling (Berendsen thermostat), with a time constant of 1 ps, was applied to maintain the reference temperature (310 K) throughout the whole run. The subsequent production step consisted of 200 ns of MD simulation in an isothermal−isobaric (*NPT*) ensemble at 1 atm and 310 K. This approach was repeated in triplicate for each system; then, 18 trajectories were run. The analysis of the MD trajectories was performed by means of VMD,[23] Chimera software,[24] together with the tools included in the GROMACS package.

To deeply investigate the antioxidant activity of the NPs, density functional theory (DFT) was used. In detail, a thermodynamic parameter, hydrogen atom transfer (HAT), was calculated for both EGCG and C18-EGCG. HAT is the transfer mechanism of a hydrogen atom from a catechin to the $OH^{\bullet}$ radical. The B3LYP hybrid functional[25] in combination with 6-311++G (d,p) basis set was used for the calculations.

2.4. Hydroxyl Radical Scavenging Assay by Electron Paramagnetic Resonance. Hydroxyl radicals ($HO^{\bullet}$) were generated by a Fenton reaction using ferrous sulfate (Fe_2SO_4) and hydrogen peroxide (H_2O_2) following the reported eq 1[26]

$$Fe^{2+} + H_2O_2 \rightarrow Fe^{3+} + OH^- + OH^{\bullet} \quad (1)$$

In the presence of 5,5-dimethyl-1-pyrroline *N*-oxide (DMPO) as a spin trap, the generated $HO^{\bullet}$ radicals were rapidly trapped to yield the corresponding $[DMPO\text{-}HO]^{\bullet}$ adduct characterized by its typical four-line EPR signal. Five mM H_2O_2 and 10 mM DMPO were added to a water solution of DNPs and PNPs (functionalized or no-functionalized with EGCG-C18) followed by the addition of 2 mM Fe_2SO_4. Free EGCG-C18 was used as a positive control at the same concentrations as the EGCG-C18 content in the PNP and DNP formulations (300 μM), while a DMPO pure solution was used as a negative control. Each recorded EPR spectrum was transformed by double integration to evaluate the total amount of radicals released after 10 min of incubation of the NPs. X-band EPR measurements were carried out on a Bruker EMX/Xenon spectrometer system equipped with a microwave frequency counter and an NMR Gaussmeter for field calibration. Quantitative estimations were performed using the native (Xenon) spectrometer software standardized with proper alanine samples. For the acquisition parameters, the modulation amplitude was settled to 1000 G, with a PTS/

https://doi.org/10.1021/acsomega.3c07637
ACS Omega 2023, 8, 48292−48303

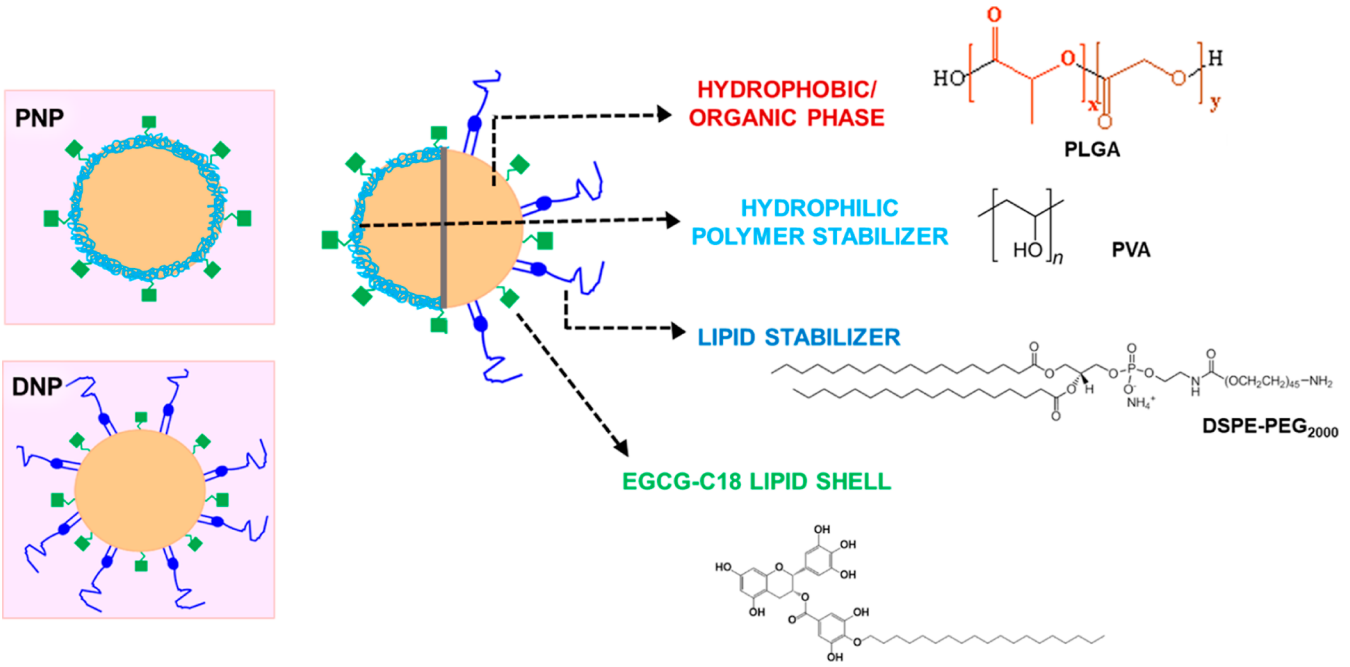

Figure 2. General antioxidant nanoparticle (NP) representation.

Table 1. Composition of Investigated PLGA/PVA NPs (PNPs) and PLGA/DSPE-PEG$_{2000}$ NPs (DNPs) in the Presence of EGCG-C18

nanoparticles (NPs)	EGCG-C18/PLGA ratio (w/w)	hydrodynamic diameter (DH) (nm)	polydispersity index (PDI)	Z potential (mV)
PNP		190 ± 5	0.07 ± 0.02	−10 ± 2
PNP-L1	1:15	210 ± 4	0.06 ± 0.02	−12 ± 5
PNP-L2	1:5	252 ± 7	0.03 ± 0.01	−9 ± 4
PNP-L3	1:2	311 ± 18	0.08 ± 0.06	−10 ± 4
DNP		112 ± 6	0.06 ± 0.02	−20 ± 4
DNP-L1	1:15	111 ± 3	0.08 ± 0.03	−22 ± 8
DNP-L2	1:5	122 ± 2	0.09 ± 0.01	−29 ± 9
DNP-L3	1:2	140 ± 4	0.07 ± 0.02	−23 ± 4

modulation amplitude of 10,000. The AutoScaling option was avoided to perform the quantitative analysis, and the receiver gain and the module frequency were settled to 30 dB and 100 MHz, respectively.

2.5. Cellular Protection Assay. For treatments, human dermal fibroblasts (HDFs) were seeded in 96-well plates at 2.5 × 10^4/well to reach 80% confluence after 24 h. Then, the medium from each well was replaced with fresh medium containing nanoformulations loaded or not loaded with EGCG-C18 (PNP, DNP, PNP-L2, and DNP-L2). The results were compared with the equal concentration of free EGCG-C18 in methanol (50 μM). After incubation for 30 min, cells were treated with H_2O_2 (1 mM) for an additional 24 h. Previous cellular viability assays were performed to establish the combination of dose/time of H_2O_2 able to induce about 40−50% of cell death after 24 h of treatment (data not shown), cytotoxicity of empty nanoparticles, and the cytotoxicity of free EGCG-C18.

2.6. Statistical Analyses. Data are presented as mean ± SD (standard deviation). Statistical comparison of differences among groups of data in both cellular experiments and EPR spectroscopy results was carried out using Student's t-test. $P \leq 0.05$ was considered statistically significant and $P \leq 0.001$ was considered highly significant.

3. RESULTS AND DISCUSSIONS

3.1. Nanoantioxidant Fabrication and Effect of EGCG-C18 on the Particle Size. The fabrication of PLGA nanoparticles engineered with EGCG-C18 was performed by using two stabilizers, PVA (PNP) and DSPE-PEG$_{2000}$ (DNP), which differently interact with the PLGA core. PVA is a water-soluble synthetic polymer stabilizing the PLGA matrix by forming a relatively compact layer surrounding the NP surface[27] (Figure 2). In the DNP, the DSPE-PEG$_{2000}$ self-assembled around the NP core, with its lipidic tail anchored to the particle core and with its hydrophilic PEG moiety facing outward in the external aqueous face, resulting in the formation of a lipid monolayer at the interface of the PLGA core covered by a PEG shell[28] (Figure 2). About the presence of DSPE-PEG$_{2000}$, the C18 hydrocarbon chain may self-assemble around the NP core via hydrophobic interactions, while the hydrophilic EGCG moiety should extend toward the aqueous phase, then leading to the formation of an antioxidant lipid shell on the NP surface (Figure 2).

The overall composition of PLGA NPs is shown in Table 1. PNP showed a particle size of about 190 nm while DNP showed a particle size of about 110 nm in hydrodynamic diameter (DH), in agreement with previously reported results in which the presence of DSPE-PEG$_{2000}$ to PLGA led to smaller NPs compared to PLGA−PVA particles.[29,30]

https://doi.org/10.1021/acsomega.3c07637
ACS Omega 2023, 8, 48292−48303

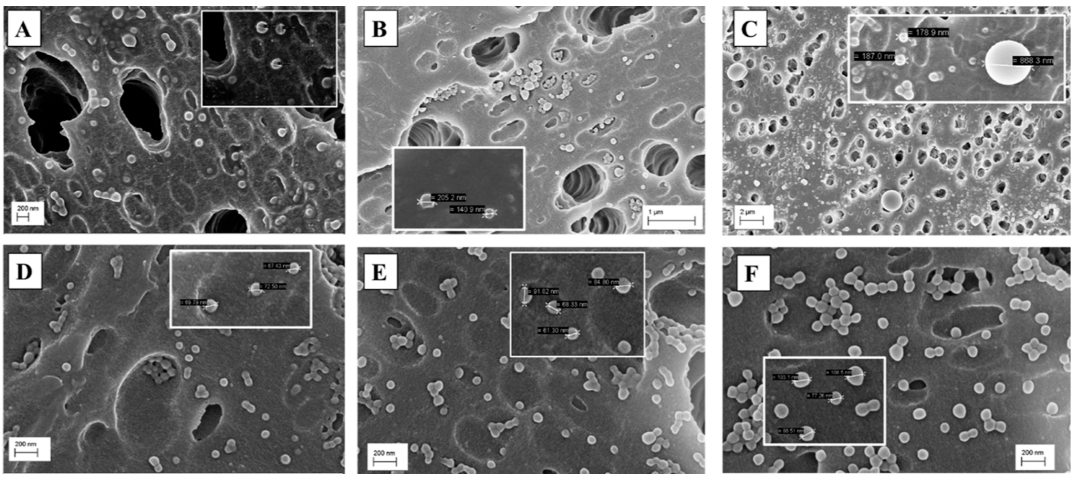

Figure 3. SEM images of PLGA nanoparticles produced in the presence of PVA and DSPE-PEG$_{2000}$ as stabilizers and analyzed after 24 h from preparation: (A) PNP, (B) PNP-L2, (C) PNP-L3, (D) DNP, (E) DNP-L2, and (F) DNP-L3.

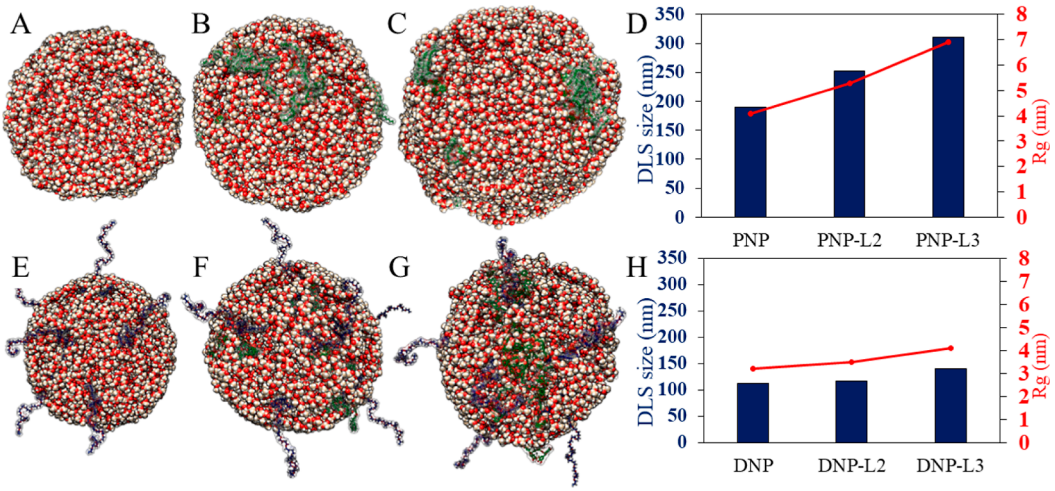

Figure 4. Representative structures of the pure PNP (A), PNP-L2 (B), PNP-L3 (C), DNP (E), DNP-L2 (F), and DNP-L3 (G). C, O, and H atoms in PLGA are reported in brown, red, and white spheres, respectively, while EGCG-C18 and PEG molecules are highlighted in green and blue, respectively. Correlation between the NP size (from DLS) (in blue) and R_g (from MD) (in red) for PNP- (D) and DNP- (H) based formulations.

The introduction of EGCG-C18 around the PNP influenced the DH of particle size in a dose-dependent way, reaching a DH of 300 nm in the EGCG-C18/PLGA ratio of 1:2 (PNP-L3), with a few precipitates clearly visible. A similar result was obtained after encapsulation of EGCG inside PLGA/PVA NPs, revealing that the aggregation phenomena was likely related to the formation of several hydrogen bonds (HBs) between EGCG and PLGA rather than the C18 alkyl chain. Instead, the DH of DNP remained almost constant and an increase of about 10 and 30 nm in particle size was observed for the DNP-L2 and DNP-L3, respectively.

SEM experiments performed on unloaded and EGCG-C18-containing NPs confirmed the DLS measurements (Table 1) and a progressive increase in the mean diameter has been found. As shown in Figure 3, in PNP-L3, there were some NPs with a particle size of about 700−800 nm (Figure 3C) while a more uniform particle size distribution was detected for all DNP formulations (Figure 3D−F).

To better understand the reason for the differences observed in the particle size, MD simulations were carried out studying the self-assembly and adsorption phenomena of EGCG-C18 on the PLGA surface both in presence and absence of DSPE-PEG$_{2000}$. MD simulations revealed that for each system, the starting dispersed polymer phase rapidly demixed into disordered droplets containing randomly oriented organic clusters. Proceeding along the MD simulations, the number of polymer droplets decreased due to their coalescence and fusion. Finally, an ordered NP is formed within the polymer nanoclusters. As the hydrophobic species associate and interact with each other, the hydrogen bonds that the monomers of the chains formed with water are broken, resulting in an increase in enthalpy (Figures 3 and 4).[31]

Focusing on the behavior of EGCG-C18, as shown in Figure 4B,C,F,G, the catechin molecules were found in peripheral regions of the PLGA polymer at the polymer/water interface, confirming the ability of modified polyphenol to form a lipid shell around the PLGA core. All systems exhibited a similar spherical morphology, in line with the SEM results. The addition of EGCG-C18 produced a concentration-dependent increase in the nanoparticle size for those prepared in the presence of PVA (Figure 4A−C). The radius of gyration (R_g), which describes how the components of NP are distributed

https://doi.org/10.1021/acsomega.3c07637
ACS Omega 2023, 8, 48292−48303

around the axis of rotation along the MD trajectories, showed high values for the PNP-based systems (Figure 4D); in addition, these values reflected dissimilar behaviors as a function of the EGCG-C18 concentration. In fact, the lowest R_g has been found for the PNP (4.9 nm), while an increase has been registered in the PNP-L2 (5.3 nm). Finally, the R_g values increased again moving to 5.9 nm for PNP-L3 systems (4.12 nm). On the other hand, the DNP-based systems exhibited smaller sizes compared to the respective PNP-based systems (Figure 4E−G); consequently, the R_g values decreased as well (Figure 4H). Small R_g values indicate that the DNPs were relatively more compact and adopted a folded structure throughout their trajectory. Despite this, an effect of the EGCG-C18 concentration has been detected again, with an increase of R_g values from 3.2 in absence of polyphenol, passing for 3.5 nm in DNP-L2, and reaching 4.1 nm for DNP-L3. Also in this case, the variations of particle sizes were reflected on the calculated R_g values. Overall, there was a high correlation between the experimental and in silico results, evidencing a reliable method to reproduce the component's self-assembly and then to predict the behavior of the resulting NPs.

3.2. Insertion Strength of EGCG-C18 Inside the PLGA Matrix. In order to understand and characterize the interactions between EGCG-C18 and the PLGA polymers, data arising from loading capacity experiments, drug release, AFT-IR measurements, and binding free energy calculations from MD simulations were considered.

The encapsulation efficiency (EE %) in all types of NPs decreased from the lower to the higher EGCG-C18 concentration (Table 2), while a progressive increase in the loading capacity (DL %) was observed. The decrease in EE % is related to the different starting concentration of EGCG-C18, while DL % directly reflects the amount of total entrapped polyphenol with respect to the total NP's weight. The DNP-L2 and DNP-L3 formulations showed a higher ability to load EGCG-C18 and the EE % was about 20% higher with respect to PNP-L2 and PNP-L3, respectively. Therefore, drug loading (DL) resulted in being much higher when DSPE-PEG_{2000} was used as a stabilizer. It is important to note that the introduction of C18 alkyl chain led to an overall higher loading capacity of polyphenol concerning no-functionalized molecule in which the DL % never exceeded 10%.[6,7] Monitoring the binding free energy of EGCG-C18 with the PLGA core along the whole MD trajectories, PNP-L2 and PNP-L3 exhibited −41.2 and −30.4 kcal/mol values, respectively, highlighting a decrease in the ΔG binding as the polyphenol increased. Interestingly, even if the trend was the same in the presence of DSPE-PEG_{2000}, the predicted values for DNP-L2 and DNP-L3 were −56.3 and −44.2 kcal/mol, respectively. Considering that the reported ΔG values are scaled per catechin molecule, this result shows that the use of DSPE-PEG_{2000} increased the interactions between PLGA and EGCG-C18, in line with the increase in the EE % measured experimentally.

Table 2. Interaction Strength of PLGA Formulations with EGCG-C18

nanoparticles (NPs)	EE %	EGCG-C18 (mM)	DL %	predicted ΔG_{bind} (kcal/mol)
PNP				
PNP-L1	98 ± 2	0.33 ± 0.02	7	
PNP-L2	65 ± 5	0.64 ± 0.3	14	−41.2
PNP-L3	53 ± 3	1 ± 0.2	23	−30.4
DNP				
DNP-L1	91 ± 2	0.3 ± 0.03	6.4	
DNP-L2	86 ± 5	0.81 ± 0.02	17	−56.3
DNP-L3	70 ± 4	1.64 ± 0.03	35	−44.2

The AFT-IR spectroscopy was used to study the interaction of PLGA polymers and EGCG-C18. The spectral trend of the PNP-L2 and PNP-L3 samples was very similar to that of the PNP sample, indicating that EGCG-C18 was efficiently incorporated by the polymer. However, the region between 1800 and 800 cm^{-1} showed the EGCG characteristic bands (Figure 5A), with an intensity that increased linearly with the concentration of the derivative. These bands were slightly displaced from the corresponding bands in the EGCG-C18 spectrum. In detail, the carbonyl stretching bands moved from 1694 to 1712 cm^{-1}, the peaks of the aromatic C=C bond shifted from 1629 and 1604 cm^{-1} to 1626 and 1602 cm^{-1}, respectively, and from 1520 to 1518 cm^{-1}, the peaks of O−H groups shifted from 1344 and 1236 cm^{-1} to 1341 and 1239 cm^{-1}, respectively, while the signals of C18 chain's C−H groups moved from 968 and 822 cm^{-1} to 962 and 841 cm^{-1}.[32] The band shift recorded with respect to the spectrum of pure EGCG-C18 was due to the interactions of the molecules with the surface functional groups of the polymeric matrix.

Analyzing the IR spectra obtained for DNP-based systems (Figure 5B) showed that a great similarity was found, suggesting an almost total incorporation of EGCG-C18 into the DNPs. Indeed, unlike what was reported for the previous samples, the characteristic bands of the polyphenol derivative detectable in the spectra of the DNP-L2 and DNP-L3 samples were only referred to the aromatic rings, i.e., the signals at 1630, 1602, 1517, and 1452 cm^{-1}. A band shift was highlighted, suggesting the onset of interactions between lipid, polyphenol, and polymer components. Interestingly, the characteristic bands of the carbonyl function and of the alkyl chain of EGCG-C18 were not observed, because of the strong apolar interactions with the polymer matrix.

The strength of the interaction of EGCG-C18 with PLGA also influences the release degree of these molecules from the NPs. In this concern, DNP showed instead a more sustained release of EGCG-C18 concerning PNP (Figure 5C), meaning that the presence of DSPE-PEG_{2000} prolonged the diffusion of the antioxidant. In this case, after 96 h, about 67% of EGCG-C18 release was observed; therefore, DNP-L2 retained 40% more polyphenol with respect to PNP-L2. This was clearly due to the stronger interactions of EGCG-C18 with NP when DSPE-PEG_{2000} was used.

3.3. Evaluation of NP's Protection toward Hydroxyl Radicals. The ability of the different NPs to act as radical scavengers was assessed by EPR spectroscopy. The Fenton reaction was used to generate a transient $^{\bullet}OH$ radical, which rapidly reacts with the spin-trap DMPO forming the [DMPO-HO]$^{\bullet}$ persistent radical adduct (Figure 6A), which is easily detectable from its characteristic four-peak EPR spectrum. The concentration of the [DMPO-HO]$^{\bullet}$ adduct was determined for each system (Figure 6B). In a control solution that did not contain any sample, a 2.2×10^{-5} M of [DMPO-HO]$^{\bullet}$ adduct was found. The EGCG-C18 lowered the amount of DMPO radical and detected of about 80% with respect to control (Figure 6B) confirming the ability of EGCG-C18 derivative to mitigate the H_2O_2-induced oxidative stress, likely acting as H-donor, hence scavenging free radicals.[8] Focusing on the PNP

https://doi.org/10.1021/acsomega.3c07637
ACS Omega 2023, 8, 48292−48303

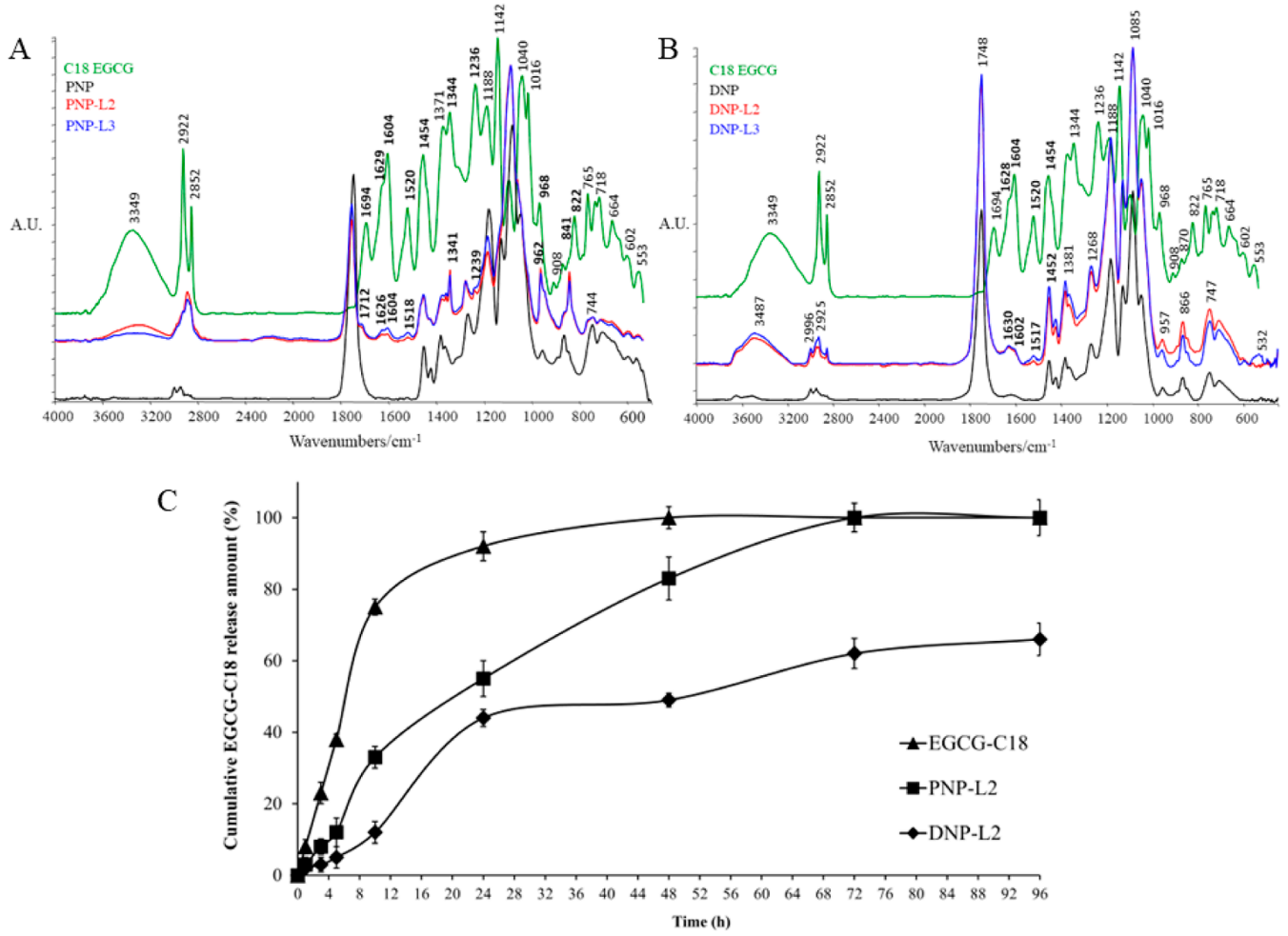

Figure 5. IR spectra of PNP- (A) and DNP- (B) based systems compared to the alone EGCG-C18 spectrum. Catechin is released from PNP-L2 and DNP-L2 (C). Values are expressed as mean ± SD; n = three independent experiments.

formulations (Figure 6C), the detected concentration of adduct was close to that found in the negative control, while a decrease of about 40% was observed in the solution containing PNP-L2. However, if compared to the results obtained using EGCG-C18 alone, it can be assessed that the presence of PLGA/PVA counteracted the scavenging activity of the polyphenol derivative.

Analyzing the EPR spectra of the DNP series, different results with respect to the previously described systems was detected. Interesting, DNP-L2 was able to completely neutralize the •OH radical (Figure 6D) showing therefore a much higher scavenging activity with respect to both PNP-L2 and EGCG-C18 alone (Figure 6E). Based on these data, DSPE-PEG_{2000} maximized the antioxidant potential of polyphenol.

To investigate in more detail the antioxidant mechanism underlying the promising capabilities found for this formulation, DFT simulations were used, and the bond dissociation enthalpy (BDE) was calculated for both EGCG and EGCG-C18 (Table 3). BDE is a thermodynamic parameter strictly correlated to the hydrogen atom transfer (HAT),[33] which is the transfer mechanism of a hydrogen atom from the catechin molecule to the OH• radical. A lower BDE is attributed to the easier transfer of the hydrogen atom from the phenolic hydroxyl group, which makes the scavenging ability of the catechin antioxidant stronger. The calculation was performed in the presence of water to show how the reaction enthalpy would be influenced by the solvent. The reason to focus on BDE is that it is known that EGCG has high free-radical scavenging capabilities, due to the ability of its pyrogallate and gallate rings (B and C rings in Figure 1) to transfer H atoms,[34,35] and that it is reasonable to compare the BDE values obtained for EGCG with those found for EGCG-C18. From our calculation, the lowest value of BDE for EGCG was observed for 3′C−OH of the B ring (300.41 kJ/mol), followed by 3″C−OH of the C ring (307.62 kJ/mol), and 2′C−OH of the B ring (331.76 kJ/mol). The 2″- and 4″C−OH of the D ring together with the 4′C−OH of the B ring had very similar increased BDE values (around 337.6 kJ/mol), and a further increase was found for the other two C−OH bonds of the benzenediol ring (A ring in Figure 1) (385.76 and 404.13 kJ/mol for 1C−OH and 3C−OH, respectively). These results indicate that the two OH groups of B and C rings in the para position are the most reactive ones for H-atom donating, in perfect concordance with the literature.[35,36]

The BDE calculation for EGCG-C18 was conducted two times, using the conformer obtained at the end of the MD simulation in DNP-L2 and in PNP-L2. The purpose of this comparison is to identify the effect of the EGCG-C18 conformation adopted in the two different formulations; since the steric effect prevails over the electronic effect, it is plausible to think that the BDEs should change a lot depending

https://doi.org/10.1021/acsomega.3c07637
ACS Omega 2023, 8, 48292−48303

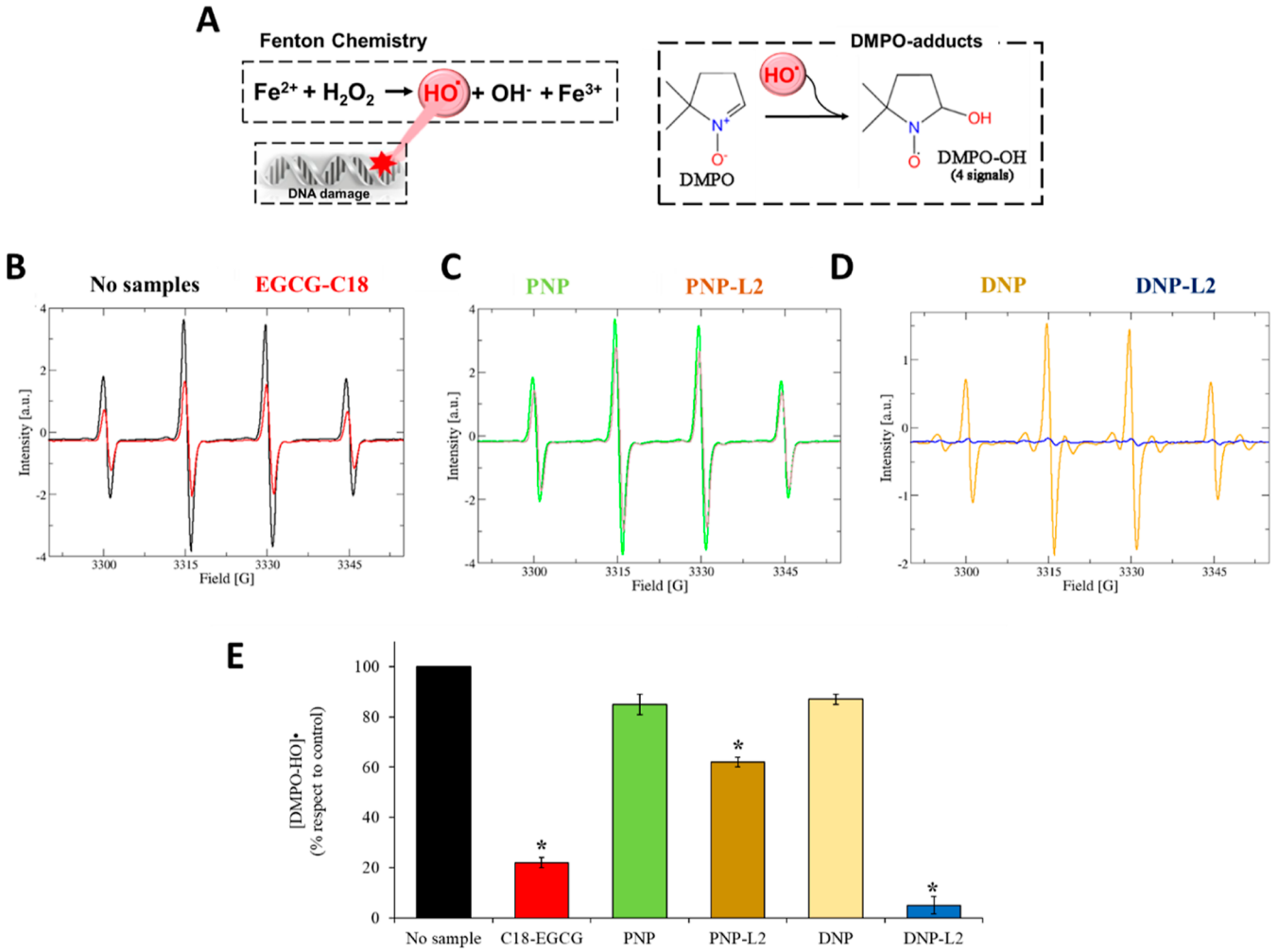

Figure 6. Fenton reaction produced a hydroxyl radical which was quantified by DMPO as a water-soluble spin trap (A). EPR spectra of negative control (black), EGCG-C18 (red) (B), PNP (green), PNP-L2 (brown) (C), DNP (orange), DNP-L2 (blue) (D). Percentage of the [DMPO-HO]• adduct with respect to control (no sample) (E). *$P < 0.001$ with respect to control.

Table 3. Calculated BDE Values for EGCG and EGCG-C18 (in kJ/mol)

groups	EGCG	EGCG-C18 (in PNP-L2)	EGCG-C18 (in DNP-L2)	ring
3′C−OH	300.41	341.67	309.77	B
2′C−OH	331.76	382.33	309.78	B
4′C−OH	337.58	375.71	348.84	B
3″C−OH	307.62			C
2″C−OH	337.61	407.60	370.98	C
4″C−OH	337.63	396.02	404.13	C
1C−OH	385.76	311.27	381.97	A
2C−OH	404.13	318.02	398.02	A

on how the aliphatic chain is arranged, thus affecting the scavenging ability of the entire molecule.

Focusing on EGCG-C18 in PNP-L2, the position of the chain close to the phenolic head induced a general increase in BDE of the OH groups placed in B and C rings and a small decrease for those in the A ring. These data confirm that the catechin derivative in PNP-L2 has a decreased scavenging activity, as demonstrated by the EPR analysis, where EGCG-C18 alone was more reactive than in the formulation.

Analysis of the BDE in DNP-L2 revealed that the main active site of EGCG-C18 was the B ring, with 3′C−OH and 2′C−OH groups (309.77 and 309.78 kJ/mol, respectively). This result reveals the possibility of EGCG-C18 to use its B ring to operate two scavenging phenomena based on HAT,[37] explaining the high scavenging activity of the catechin derivative in this conformation. An increase in BDE was observed for the 4′C−OH of the B ring (348.84 kJ/mol) and the 2″C−OH and 4″C−OH groups of the C ring (370.98 and 404.13 kJ/mol). This is not a surprise since the BDE increase in the C ring is correlated to the lipophilic derivatization; in fact, the same was observed in PNP-L2. Finally, in line with the observation on EGCG, a further increase was found for the other two C−OH bonds of the A ring (381.97 and 398.02 kJ/mol for 1C−OH and 3C−OH, respectively).

3.4. Molecular Organization of EGCG-C18 Influenced the Radical Scavenging Activity of the Nanoantioxidant. To explain and understand how the two different stabilizers impact the scavenging activity of nanomaterial, the molecular organization of EGCG-C18 on the PLGA surface was studied by MD simulations. Mass density profiles of PLGA and EGCG-C18 without and with DSPE-PEG_{2000} were examined. In the absence of DSPE-PEG_{2000}, the EGCG-C18 remained close to the polymeric surface, although inside it (Figure 7A); conversely, when the lipid stabilizer was present, the EGCG-C18 appeared to settle above the polymer surface

https://doi.org/10.1021/acsomega.3c07637
ACS Omega 2023, 8, 48292−48303

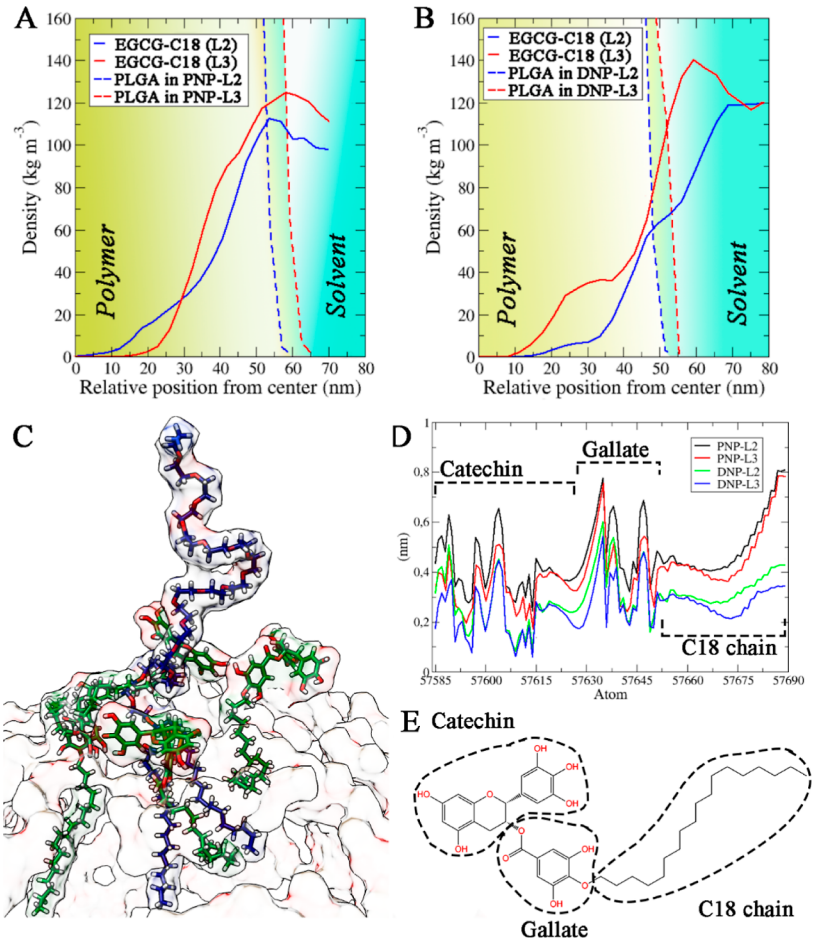

Figure 7. Mass density profiles of PLGA and the EGCG-C18 lipid in PNP (A) and DNP (B). These plots report the average distances from the PLGA center considering the *x*, *y*, and *z* axes. Representative structure of EGCG-C18 molecules surrounding DSPE-PEG$_{2000}$ (C); in both pictures, lipid, catechin, and polymer are reported in blue sticks, green sticks, and transparent surfaces, respectively. Average root-mean-square fluctuations (D) and 2D structure (E) of EGCG-C18.

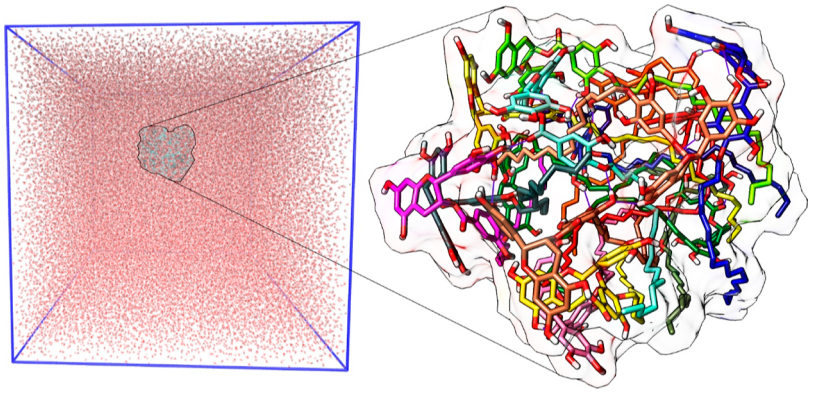

Figure 8. EGCG-C18 molecules in a simulation box with water. In the focus of the aggregate, each catechin molecule is reported in different colors. The small lines between the molecules represent the H bonds, while the H atoms have not been highlighted to improve clarity.

exposing parts of the hydrophilic head to the solvent (Figure 7B). Therefore, the role of DSPE-PEG$_{2000}$ in the interaction of EGCG-C18 with the PLGA matrix was deeply studied. When included, the DSPE lipid was always located orienting their stearoyl parts toward the PLGA core, while the long polar chains of PEG moiety were located outside the polymer system, maximizing the interactions with the water molecules. The DSPE-PEG$_{2000}$ molecules appeared homogeneously distributed in the peripheral parts of the polymer, showing no interactions between them. The aliphatic chain of EGCG-C18 molecules strongly interact with those of DSPE-PEG$_{2000}$ (Figure 7C), leading to self-assembling of EGCG-C18 near the DSPE-PEG$_{2000}$ on the PLGA surface. Therefore, these apolar interactions oriented the polyphenolic heads toward the solvent, thus offering the maximum degree of protection from OH radicals. The direct interactions between these components were also observed monitoring the root-mean-square fluctuations (RMSFs) of EGCG-C18 (Figure 7D). The

https://doi.org/10.1021/acsomega.3c07637
ACS Omega 2023, 8, 48292−48303

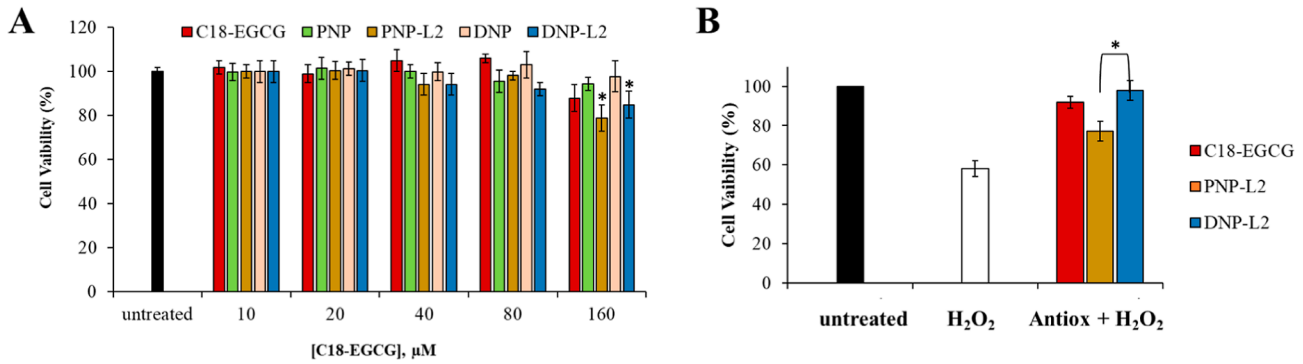

Figure 9. (A) Cytotoxicity of free EGCG-C18, PNP, DNP, PNP-L2, and DNP-L2 after 48 h of treatment. *$P < 0.05$ with respect to untreated cells. (B) Effect of free EGCG-C18 and EGCG-C18 integrated in the PLGA NP in HDF cells after H_2O_2 exposure by MTT assay. The cells were pretreated with 40 μM of free EGCG-C18 or PNP-L2 and DNP-L2 for 30 min, before being exposed to 1 mM H_2O_2 for 24 h. Every set of data represents three experiments with five replicates for each condition tested. *$P < 0.05$, PNP-L2 vs DNP-L2.

data reported are averaged values considering all MD trajectories. The portion of the molecule between atoms 57,585 and 57,615 is constituted by the catechin moiety, the atoms 57,630−57,650 by the gallate part, and the whole final segment is relative to the C18 chain (Figure 7E). DSPE-PEG_{2000} decreased the fluctuation degree of EGCG-C18 molecules, and by focusing on the single components, an evident fluctuation loss was detected for the C18 chains in DNP-L2 and DNP-L3 systems. This behavior was concentration dependent and was clearly given by the high apolar interactions between EGCG-C18 and DSPE-PEG_{2000}.

In the absence of DSPE-PEG_{2000}, high clusterization of EGCG-C18 on the PLGA surface was found (Figure 4B,C); in this context, the hydroxyl groups of EGCG moiety, which is responsible for the H-donating process, could result as partially hidden.

Finally, to explain why EGCG-C18 showed stronger scavenging activity against $^{\bullet}$OH radicals when it was included in DNP, proper MD simulation of free EGCG-C18 was performed. The MD trajectories showed that the polyphenol derivative molecules aggregated very quickly, decreasing the number of interactions with the solvent (Figure 8).

More in detail, hydrogen bonds (H bonds) between the OH groups and π-stacking interactions between the aromatic heads were observed; moreover, strong apolar interactions were observed between the long aliphatic chains, which tended to fold on themselves to favor a greater number of hydrophobic contacts. This resulted in the formation of a disordered aggregate, with the polyphenolic heads exposed more toward the solvent. No order displacement was observed, meaning that the polyphenolic components were always grouped between them. An average number of 20 H bonds between the EGCG-C18 molecules was detected along the MD simulations, and this intrinsic behavior to stably aggregate means that the protection capabilities of the catechin derivative toward $^{\bullet}$OH radicals will be less in the absence of DSPE-PEG_{2000}; therefore, the use of this lipid stabilizer represents a winning choice to create an effective and stable polyphenol-based nanoantioxidant.

3.5. Nanoantioxidant Protection of Human Dermal Fibroblasts from Oxidative Stress-Induced Cell Death. The effective ability of NPs to protect cells from oxidative damage was assessed in human dermal fibroblasts which are cells frequently subjected in vivo to high free radicals exposure. Based on cytotoxic studies (Figure 9A), we selected 40 μM of EGCG-C18 concentration, which did not induce a decrease in cellular viability after 48 h of treatment. The pretreatment with both PNP-L2 and PNP-L2 significantly increased cell survival with respect to H_2O_2-treated cells although with different efficacies (Figure 9B). DNP-L2 provided a cellular protection of about 20% higher concerning PNP-L2. No significative differences were observed between the effects of free EGCG-C18 and DNP-L2 formulation; however, it is important to underline that the lipophilic nature of the EGCG derivative makes it a poorly water-soluble drug that required an organic solvent to be administered.[6]

4. CONCLUSIONS

In this work, PLGA NPs engineered with a lipid-functionalized EGCG were studied in the presence of two different stabilizers, PVA and DSPE-PEG_{2000}. A combined computational-experimental approach was used to successfully design and fabricate the antioxidant nanomaterial, thus leading to the explanation of the role of each constituent used and to find out the optimal condition to maximize the biological activity of EGCG-C18. Overall, the use of DSPE-PEG_{2000} as a lipid stabilizer showed several advantages for developing an optimal polyphenol-based PLGA nanoantioxidant. It led to the formation of small NPs of about 100 nm able to encapsulate a very large amount of antioxidant EGCG-C18. Moreover, the presence of DSPE-PEG_{2000} induces EGCG-C18 to orient its polyphenolic head at the polymer−solvent interface increasing the radical scavenging activity in aqueous solution. This trend was confirmed by the evaluation of the capability of different NPs to protect human dermal fibroblasts from oxidative stress-induced cell death, showing that DNP-L2 exhibited the highest protection.

From the results obtained, DNP-L2 represents a novel polyphenol-based material that could be used for several applications, from multifunctional drug delivery to tissues.

AUTHOR INFORMATION

Corresponding Author

Emiliano Laudadio − *Department of Science and Engineering of Matter, Environment and Urban Planning, Polytechnic University of Marche, 60121 Ancona, Italy;* orcid.org/0000-0002-8053-6539; Email: e.laudadio@staff.univpm.it

https://doi.org/10.1021/acsomega.3c07637
ACS Omega 2023, 8, 48292−48303

Authors

Cristina Minnelli − *Department of Life and Environmental Science, Polytechnic University of Marche, 60121 Ancona, Italy;* orcid.org/0000-0001-8034-8557

Pierluigi Stipa − *Department of Science and Engineering of Matter, Environment and Urban Planning, Polytechnic University of Marche, 60121 Ancona, Italy;* orcid.org/0000-0001-9024-0398

Giovanna Mobbili − *Department of Life and Environmental Science, Polytechnic University of Marche, 60121 Ancona, Italy*

Simona Sabbatini − *Department of Science and Engineering of Matter, Environment and Urban Planning, Polytechnic University of Marche, 60121 Ancona, Italy*

Brenda Romaldi − *Department of Clinical Sciences, Polytechnic University of Marche, 60121 Ancona, Italy*

Tatiana Armeni − *Department of Clinical Sciences, Polytechnic University of Marche, 60121 Ancona, Italy*

Complete contact information is available at: https://pubs.acs.org/10.1021/acsomega.3c07637

Notes

The authors declare no competing financial interest.

■ ACKNOWLEDGMENTS

This research was partially funded by the European Union's Next Generation EU. Project Code: ECS00000041; Project Title: "Innovation, digitalization and sustainability for the diffused economy in Central Italy—VITALITY". The authors would like to acknowledge the CINECA-HPC ISCRA MARCONI-100 computer system (ATOM-HMV project no. HP10CEE3EH) for the calculations on GROMACS.

■ REFERENCES

(1) Brito, J.; Hlushko, H.; Abbott, A.; Aliakseyeu, A.; Hlushko, R.; Sukhishvili, S. A. Integrating Antioxidant Functionality into Polymer Materials: Fundamentals, Strategies, and Applications. *ACS Appl. Mater. Interfaces* **2021**, *13* (35), 41372−41395.

(2) Minnelli, C.; Moretti, P.; Fulgenzi, G.; Mariani, P.; Laudadio, E.; Armeni, T.; Galeazzi, R.; Mobbili, G. A Poloxamer-407 Modified Liposome Encapsulating Epigallocatechin-3-Gallate in the Presence of Magnesium: Characterization and Protective Effect against Oxidative Damage. *Int. J. Pharm.* **2018**, *552*, 225−234.

(3) Baghirova, L.; Kaya Tilki, E.; Öztürk, A. A. Evaluation of Cell Proliferation and Wound Healing Effects of Vitamin A Palmitate-Loaded PLGA/Chitosan-Coated PLGA Nanoparticles: Preparation, Characterization, Release, and Release Kinetics. *ACS Omega* **2023**, *8*, 2658.

(4) Hosseininasab, S.; Pashaei-Asl, R.; Khandaghi, A. A.; Nasrabadi, H. T.; Nejati-Koshki, K.; Akbarzadeh, A.; Joo, S. W.; Hanifehpour, Y.; Davaran, S. *Retracted*: Synthesis, Characterization, and *In vitro* Studies of PLGA−PEG Nanoparticles for Oral Insulin Delivery. *Chem. Biol. Drug Des.* **2014**, *84* (3), 307−315.

(5) Wang, Y.; Qin, B.; Xia, G.; Choi, S. H. FDA's Poly (Lactic-Co-Glycolic Acid) Research Program and Regulatory Outcomes. *AAPS J.* **2021**, *23* (4), 92.

(6) Minnelli, C.; Stipa, P.; Sabbatini, S.; Mengucci, P.; Mobbili, G.; Galeazzi, R.; Armeni, T.; Romaldi, B.; Celli, A.; Laudadio, E. Insights into PLGA-Encapsulated Epigallocatechin 3-Gallate Nanoparticles as a New Potential Biomedical System: A Computational and Experimental Approach. *Eur. Polym. J.* **2023**, *182*, 111723.

(7) Srivastava, A. K.; Bhatnagar, P.; Singh, M.; Mishra, S.; Kumar, P.; Shukla, Y.; Gupta, K. C. Synthesis of PLGA Nanoparticles of Tea Polyphenols and Their Strong in Vivo Protective Effect against Chemically Induced DNA Damage. *Int. J. Nanomed.* **2013**, *8*, 1451−1462.

(8) Minnelli, C.; Galeazzi, R.; Laudadio, E.; Amici, A.; Rusciano, D.; Armeni, T.; Cantarini, M.; Stipa, P.; Mobbili, G. Monoalkylated Epigallocatechin-3-Gallate (C18-EGCG) as Novel Lipophilic EGCG Derivative: Characterization and Antioxidant Evaluation. *Antioxidants* **2020**, *9* (3), 208.

(9) Kurita, I.; Maeda-Yamamoto, M.; Tachibana, H.; Kamei, M. Antihypertensive Effect of Benifuuki Tea Containing O-Methylated EGCG. *J. Agric. Food Chem.* **2010**, *58* (3), 1903−1908.

(10) Zhong, Y.; Shahidi, F. Lipophilized Epigallocatechin Gallate (EGCG) Derivatives as Novel Antioxidants. *J. Agric. Food Chem.* **2011**, *59* (12), 6526−6533.

(11) Marano, S.; Minnelli, C.; Ripani, L.; Marcaccio, M.; Laudadio, E.; Mobbili, G.; Amici, A.; Armeni, T.; Stipa, P. Insights into the Antioxidant Mechanism of Newly Synthesized Benzoxazinic Nitrones: In Vitro and in Silico Studies with Dpph Model Radical. *Antioxidants* **2021**, *10* (8), 1224.

(12) JC Bose, R.; Lee, S. H.; Park, H. Lipid Polymer Hybrid Nanospheres Encapsulating Antiproliferative Agents for Stent Applications. *J. Ind. Eng. Chem.* **2016**, *36*, 284−292.

(13) Bose, R. J.; Arai, Y.; Ahn, J. C.; Park, H.; Lee, S. H. Influence of Cationic Lipid Concentration on Properties of Lipid-Polymer Hybrid Nanospheres for Gene Delivery. *Int. J. Nanomed.* **2015**, *10*, 5367−5382.

(14) Minnelli, C.; Moretti, P.; Laudadio, E.; Gerelli, Y.; Pigozzo, A.; Armeni, T.; Galeazzi, R.; Mariani, P.; Mobbili, G. Tuning Curvature and Phase Behavior of Monoolein Bilayers by Epigallocatechin-3-Gallate: Structural Insight and Cytotoxicity. *Colloids Surf., B* **2022**, *209*, 112171.

(15) Stipa, P.; Marano, S.; Galeazzi, R.; Minnelli, C.; Laudadio, E. Molecular Dynamics Simulations of Quinine Encapsulation into Biodegradable Nanoparticles: A Possible New Strategy against Sars-CoV-2. *Eur. Polym. J.* **2021**, *158*, 110685.

(16) Jakalian, A.; Jack, D. B.; Bayly, C. I. Fast, Efficient Generation of High-Quality Atomic Charges. AM1-BCC Model: II. Parameterization and Validation. *J. Comput. Chem.* **2002**, *23* (16), 1623−1641.

(17) Mark, P.; Nilsson, L. Structure and Dynamics of the TIP3P, SPC, and SPC/E Water Models at 298 K. *J. Phys. Chem. A* **2001**, *105* (43), 9954−9960.

(18) Abraham, M. J.; Murtola, T.; Schulz, R.; Páll, S.; Smith, J. C.; Hess, B.; Lindahl, E. Gromacs: High Performance Molecular Simulations through Multi-Level Parallelism from Laptops to Supercomputers. *SoftwareX* **2015**, *1−2*, 19−25.

(19) Van Der Spoel, D.; Lindahl, E.; Hess, B.; Groenhof, G.; Mark, A. E.; Berendsen, H. J. C. GROMACS: Fast, Flexible, and Free. *J. Comput. Chem.* **2005**, *26* (16), 1701−1718.

(20) Yu, Y.; Krämer, A.; Venable, R. M.; Brooks, B. R.; Klauda, J. B.; Pastor, R. W. CHARMM36 Lipid Force Field with Explicit Treatment of Long-Range Dispersion: Parametrization and Validation for Phosphatidylethanolamine, Phosphatidylglycerol, and Ether Lipids. *J. Chem. Theory Comput.* **2021**, *17* (3), 1581−1595.

(21) Laudadio, E.; Galeazzi, R.; Mobbili, G.; Minnelli, C.; Barbon, A.; Bortolus, M.; Stipa, P. Depth Distribution of Spin-Labeled Liponitroxides within Lipid Bilayers: A Combined EPR and Molecular Dynamics Approach. *ACS Omega* **2019**, *4* (3), 5029−5037.

(22) Hess, B.; Bekker, H.; Berendsen, H. J. C.; Fraaije, J. G. E. M. LINCS: A Linear Constraint Solver for Molecular Simulations. *J. Comput. Chem.* **1997**, *18*, 1463−1472.

(23) Zhang, R.; Gao, C.; Pan, S.; Shang, R. Fusion of GNSS and Speedometer Based on VMD and Its Application in Bridge Deformation Monitoring. *Sensors* **2020**, *20* (3), 694.

(24) Pettersen, E. F.; Goddard, T. D.; Huang, C. C.; Couch, G. S.; Greenblatt, D. M.; Meng, E. C.; Ferrin, T. E. UCSF Chimera - A Visualization System for Exploratory Research and Analysis. *J. Comput. Chem.* **2004**, *25* (13), 1605−1612.

(25) Anitha, S.; Krishnan, S.; Senthilkumar, K.; Sasirekha, V. Theoretical Investigation on the Structure and Antioxidant Activity of

(+) Catechin and (−) Epicatechin-a Comparative Study. *Mol. Phys.* **2020**, *118* (17), No. e1745917.
(26) Morales, N. P.; Sirijaroonwong, S.; Yamanont, P.; Phisalaphong, C. Electron Paramagnetic Resonance Study of the Free Radical Scavenging Capacity of Curcumin and Its Demethoxy and Hydrogenated Derivatives. *Biol. Pharm. Bull.* **2015**, *38* (10), 1478−1483.
(27) Ramirez, J. C.; Flores-Villaseñor, S. E.; Vargas-Reyes, E.; Herrera-Ordonez, J.; Torres-Rincón, S.; Peralta-Rodríguez, R. D. Preparation of PDLLA and PLGA Nanoparticles Stabilized with PVA and a PVA-SDS Mixture: Studies on Particle Size, Degradation and Drug Release. *J. Drug Delivery Sci. Technol.* **2020**, *60*, 101907.
(28) Rashighi, M.; Harris, J. E. *Physiol. Behav.* **2017**, *176* (3), 139−148.
(29) Albert, C.; Huang, N.; Tsapis, N.; Geiger, S.; Rosilio, V.; Mekhloufi, G.; Chapron, D.; Robin, B.; Beladjine, M.; Nicolas, V.; Fattal, E.; Agnely, F. Bare and Sterically Stabilized PLGA Nanoparticles for the Stabilization of Pickering Emulsions. *Langmuir* **2018**, *34* (46), 13935−13945.
(30) Bao, Y.; Maeki, M.; Ishida, A.; Tani, H.; Tokeshi, M. Preparation of Size-Tunable Sub-200 Nm PLGA-Based Nanoparticles with a Wide Size Range Using a Microfluidic Platform. *PLoS One* **2022**, *17* (8), No. e0271050.
(31) Yuan, C.; Levin, A.; Chen, W.; Xing, R.; Zou, Q.; Herling, T. W.; Challa, P. K.; Knowles, T. P. J.; Yan, X. Nucleation and Growth of Amino Acid and Peptide Supramolecular Polymers through Liquid-Liquid Phase Separation. *Angew. Chem., Int. Ed.* **2019**, *58* (50), 18116−18123.
(32) Radhakrishnan, R.; Kulhari, H.; Pooja, D.; Gudem, S.; Bhargava, S.; Shukla, R.; Sistla, R. Encapsulation of Biophenolic Phytochemical EGCG within Lipid Nanoparticles Enhances Its Stability and Cytotoxicity against Cancer. *Chem. Phys. Lipids* **2016**, *198*, 51−60.
(33) Rittle, J.; Peters, J. C. N-H Bond Dissociation Enthalpies and Facile H Atom Transfers for Early Intermediates of Fe-N2 and Fe-CN Reductions. *J. Am. Chem. Soc.* **2017**, *139* (8), 3161−3170.
(34) Wang, Z.; Liu, Z.; Wu, C.; Liu, S.; Wang, D.; Hu, C.; Chen, T.; Ran, Z.; Gan, W.; Li, G. Computational Analysis on Antioxidant Activity of Four Characteristic Structural Units from Persimmon Tannin. *Materials* **2023**, *16* (1), 320.
(35) Wang, J.; Tang, H.; Hou, B.; Zhang, P.; Wang, Q.; Zhang, B. L.; Huang, Y. W.; Wang, Y.; Xiang, Z. M.; Zi, C. T.; Wang, X. J.; Sheng, J. Synthesis, Antioxidant Activity, and Density Functional Theory Study of Catechin Derivatives. *RSC Adv.* **2017**, *7* (85), 54136−54141.
(36) Boulmokh, Y.; Belguidoum, K.; Meddour, F.; Amira-Guebailia, H. Investigation of Antioxidant Activity of Epigallocatechin Gallate and Epicatechin as Compared to Resveratrol and Ascorbic Acid: Experimental and Theoretical Insights. *Struct. Chem.* **2021**, *32* (5), 1907−1923.
(37) Zafar, S.; Ahmed, R.; Khan, R. Biotransformation: A Green and Efficient Way of Antioxidant Synthesis. *Free Radical Res.* **2016**, *50* (9), 939−948.

https://doi.org/10.1021/acsomega.3c07637
ACS Omega 2023, 8, 48292−48303